Miner Petrol (2013) 107:327–340
DOI 10.1007/s00710-012-0255-1

ORIGINAL PAPER

# The formation of phosphoran olivine and stanfieldite from the pyrometamorphic breakdown of apatite in slags from a prehistoric ritual immolation site (Goldbichl, Igls, Tyrol, Austria)

**Philipp Schneider · Peter Tropper · Reinhard Kaindl**

Received: 11 April 2012 / Accepted: 27 November 2012 / Published online: 29 December 2012


**Abstract** In this study we report P-rich olivine and the tric-calcium phosphate (TCP) stanfieldite in partially molten quartz-phyllites from the ritual immolation site at the Goldbichl, near Innsbruck in the Tyrol, Austria. During partial melting, foamy patches of dark glassy material formed at the surface of the rocks and also as layers within the rocks. The pyrometamorphic rocks contain mostly the mineral assemblage olivine + ortho-pyroxene + plagioclase + spinel + glass. During the investigation of slag samples from this prehistoric ritual immolation site, extremely P-rich, apatite-bearing micro-domains were found. In these domains phosphoran olivine was found whose P contents are approaching the maximum P contents in olivine according to the experimental investigations of Boesenberg and Hewins (Geochim Cosmochim Acta 74:1923–1941, 2010). The textures within these domains indicate strongly disequilibrium conditions. The phosphoran olivines formed due to reactions involving apatite and the mineral assemblage of the quartzphyllites, and coexist with plagioclase and a tri-calcium phosphate phase (TCP) showing stanfieldite $Ca_4(Mg, Fe^{2+}, Mn^{2+})_5(PO_4)_6$ composition. In terms of its chemical composition, olivine shows a wide range in composition with P ranging from 0.3 to 0.54 a.p.f.u, which corresponds to maximal 23 wt.% $P_2O_5$. These are the highest P-contents in olivine reported from rocks so far. The incorporation of P correlates with decreasing Si contents according to the charge balancing scheme $2P^{5+} + M_{1,2} = 2Si^{4+} + (Mg, Fe)^{2+}M_{1,2}$. Therefore P can only be incorporated in combination with a vacancy on the $M_{1,2}$ position. Micro-Raman spectroscopy of phosphoran olivines indicates that these olivines can easily be identified with this method due to the strong signals of the $SiO_4$ and $PO_4$ vibrations. The external vibrations of the $M_{1,2}$ sites at low wave-numbers are more complex than for P-free olivine. This might be due to the effect of $P^{5+}$ on the $M_1{}^{2+}$ and $M_2{}^{2+}$ positions and the formation of vacancies on these sites. Since micro-Raman investigations of the TCP phase yielded no conclusive match with a known Raman spectrum of a phosphate mineral so far, therefore it is most likely that the TCP phase is stanfieldite, whose Raman spectrum has not been obtained yet. Schematical Schreinemakers analysis in the system $CaO$-$Al_2O_3$-$FeO$-$SiO_2$-$P_2O_5$-$H_2O$ shows that P-rich olivine (fayalite-sarcopside solid solution) can form from mineral reactions involving chlorite, apatite and quartz and show that the occurrence of P-rich Fe-olivines spans a large *T*-range but is restricted to domains with high $aSiO_2$. The mineral assemblage in the P-rich micro-domains shows that the formation of phosphoran olivine is not only restricted to the interaction between bone material and rocks in slags from ritual immolation sites as suggested by Tropper et al. (Eur J Mineral 16:631–640, 2004) from the immolation site in Oetz but can form locally due to the pyro-metamorphic breakdown of a P-rich accessory precursor phase such as apatite.

Editorial handling: A. Beran

Dedicated to Prof. Josef Zemann on the occasion of his 90th birthday

P. Schneider · P. Tropper (✉)
Institute of Mineralogy and Petrography, University of Innsbruck,
Innrain 52f, 6020, Innsbruck, Austria
e-mail: peter.tropper@uibk.ac.at

R. Kaindl
MATERIALS – Institute for Surface Technologies and Photonics,
Joanneum Research, Leobner Straße 94,
8712, Niklasdorf, Austria

## Introduction

The occurrence of phosphoran olivine with significant phosphorus contents (>2 wt.% $P_2O_5$) has been reported from only a

few places of the world (see Tropper et al. 2004). Phosophoran olivines are reported from terrestrial and extraterrestrial sources such as a syenitic breccia pipe from Pine Canyon, Utah (Agrell et al. 1998) or olivines and pyroxens from Disko Island, Greenland (Goodrich 1984), and Pallasite meteorites (Buseck and Clark 1984). The terrestrial phosphoran olivines commonly occur together with farringtonite and/or stanfieldite (Agrell et al. 1998). In contrast, experimental investigations by Boesenberg et al. (2004) and Boesenberg and Hewins (2010) yielded phosphoran olivines with up to 27 wt.% $P_2O_5$. Because of the similarity of crystal chemical properties of P and Si (low cation radius, highly charged) both occupy preferentially the tetrahedral site. Synthetic olivines with slightly elevated phosphorus contents (<1 wt.% $P_2O_5$) are known from blast furnace slags from modern, prehistoric and medieval smelting operations (Müller et al. 1988: Heimann et al. 1998) and phosphoran olivines with up to 10.5 wt.% $P_2O_5$ were reported from wrought iron from the USS Monitor (Boesenberg 2006). Phosphoran olivines also occur in pyrometamorphic slags and Tropper et al. (2004) reported the unusual occurrence of extremely phosphorus-rich olivines containing up to 8.8 wt.% $P_2O_5$ in partially molten biotite-plagioclase-gneisses recovered from the ritual immolation site Oetz in the Ötz Valley, Northern Tyrol, Austria.

Prehistoric ritual immolation sites in the Alpine area have been investigated for the past 40 years. Weiss (1997) showed that due to the lack of surface characteristics, ritual burning sites are very hard to identify and indeed their identification is mainly accidental. Weiss (1997) mentions about 120 burning sites from an area extending between the Alps and the Danube, which probably represents a lower limiting number of the actual sites. A more recent study by Gleirscher et al. (2002) extended the number of ritual immolation sites to 200 in the Alps. These sites were identified on the presence of pottery-, metal- and bone fragments and none of the sites from his investigation has ever been investigated from a mineralogical point of view, since characteristic P-bearing minerals can form due to the interaction between bone material and rocks in the course of the immolation process (Tropper et al. 2004, 2006). Prehistoric immolation sites associated with the presence of slags are mainly known from two localities in the Tyrol, namely the Goldbichl near Innsbruck and one site in Oetz in the Ötz valley approximately 50 km W of Innsbruck (Tropper et al. 2004). In both areas, the site is always on top of a hill. Von Chlingensperg (1904) was the first to interpret these sites as localities where ritual immolations took place, based in part on the abundant presence of bone fragments of domestic animals such as cow, sheep, goat and pig (Weiss 1997; Tomedi and Nicolussi Castellan 2000). Tropper et al. (2004) investigated slags from the burning site at Oetz and concluded, based on experiments using natural animal bones (Tropper et al. 2006), that mineralogical observations such as the assemblage phosphorus-rich olivine + whitlockite can indeed provide possible evidence for the burning of bone material and thus be very helpful in the identification of prehistoric immolation sites in cases where clear archeological evidence is lacking.

In this study we describe a different extremely P-rich mineral assemblage from the ritual immolation site at the Goldbichl near Igls, where quartzphyllites instead of biotite-plagioclase gnesisses (as in Oetz) were transformed into slags by anthropogenically-induced pyrometamorphism.

## Archaeological setting

The immolation site of this study is on top of the Goldbichl, a small hill a few kilometers to the S of Innsbruck near the village of Igls (Fig. 1). The Goldbichl has been used as a prehistoric cult site since the Neolithic Age (Tomedi and Nicolussi Castellan 2000). In the Early Bronze Age (1900–1650 BC) it gained importance as an immolation place. In the process of these ritual immolations bovines, goats and sheep were sacrificed on a stepped altar made of loam and rocks. Due to a natural air draft huge fires were inflamed, so that the fire could easily be seen from far away (Tomedi and Nicolussi Castellan 2000). The immolation fires were set on a circular place on the loamy ground. Only later stone altars were built. Archaeological excavations yielded fractions of ceramic vessels that contained libations. Libations are offerings of liquids and vessels that were sacrificed during these rituals. After every ritual immolation the place was cleaned and the precious sacrificial offerings were carried to a secret depot. After a long period of neglect, immolation activity started again at this site during the Iron Age (ca. 450–15 BC) according to Tomedi and Nicolussi Castellan (2000).

## Geological setting

The stones for the altar were taken locally from the area around the Goldbichl. Geologically the Goldbichl is situated in the westernmost Innsbruck Quartzphyllite complex, which is part of the Austroalpine basement nappes north of the Tauern Window (Fig. 1). The polymetamorphic Austroalpine basement consists in the vicinity of Innsbruck of lower Ordovician porphyroid gneisses (Kellerjochgneiss or Schwazer Augengneiss) micaschists (Patscherkofel and Glungezer Crystalline Complex) and Paleozoic schists (Innsbruck Quartzphyllite complex and Wildschönau Schists) with intercalated carbonates (Piber 2005). Haditsch and Mostler (1982) were the first to accomplish a serial differentiation of the Innsbruck Quartzphyllite complex. According to their division the stratigraphical lowest part consists of a greenschist-quartzphyllite series. It is

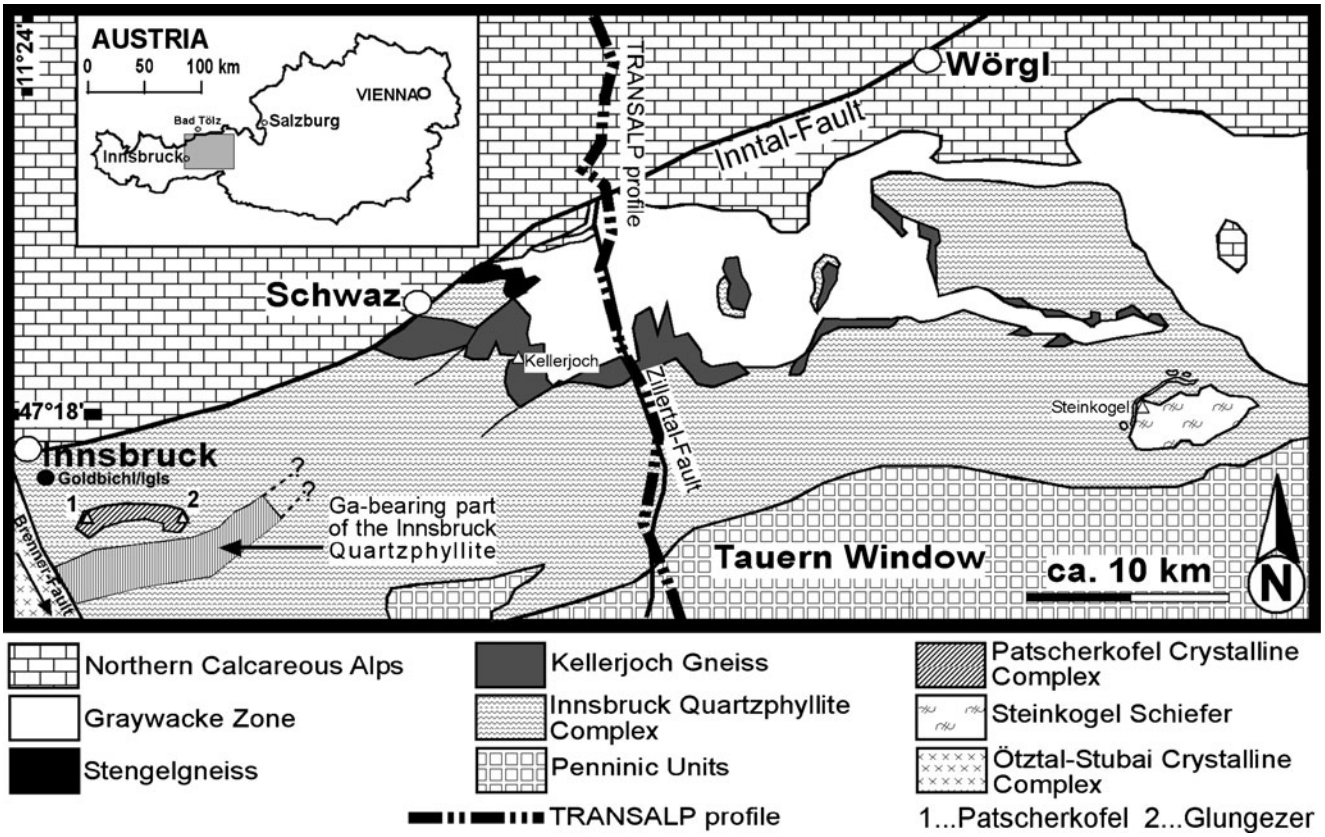


**Fig. 1** Geological overview of the lower Inn valley from Piber (2005). The location of the Goldbichl/Igls is indicated with a black circle on the left side of the map. Most of the Innsbruck Quartzphyllite consists of monotonous quartzphyllites and schists but in the western part of the Innsbruck Quartzphyllite a central garnet (Ga)-bearing zone occurs

composed of quartzphyllites and intercalated metabasic rocks. In a stratigraphically higher position the Silurian carbonate-sericite series occurs. It is composed of sericitic phyllites, quartzphyllites and chlorite-sericite-phyllites occasionally intercalated with carbonate and dolomite marbles. On top the blackschist-carbonate series and garnet-bearing phyllites intercalated with Devonian dolomite marbles occur.

## Petrography and textural relations

*Innsbruck quartzphyllite* The westernmost Innsbruck Quartzphyllite complex consists of metapsammites and metapelites. The mineral assemblage of the protolith quartzphyllites consists of muscovite + chlorite + plagioclase + quartz ± apatite ± biotite ± garnet ± clinozoisite ± ilmenite ± rutile ± titanite (Fig. 2). Titanite is the most abundant Ti-mineral and quartz and feldspar contents are highly variable and chlorite, muscovite and if present biotite form the penetrative foliation.

*Slags* The rocks of the immolation place show signs of a strong thermal overprint, which often differs on a cm scale. The samples show foamy textures as well as thin (< 0.5 cm) layers of glass. The foamy patches show a diamter of < 3 cm

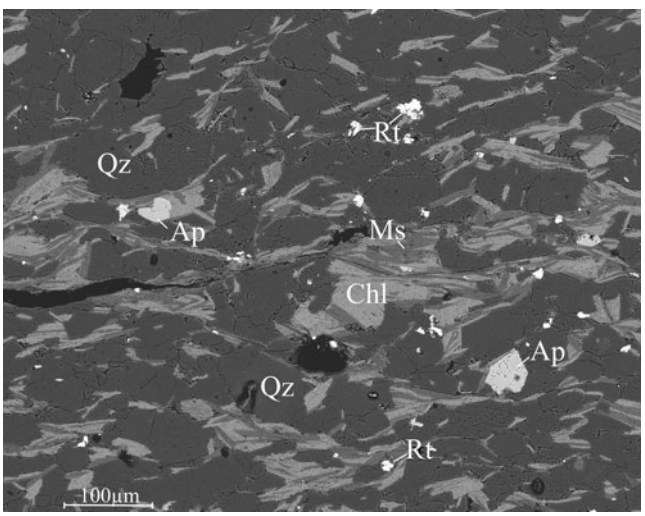


**Fig. 2** BSE image of a sample of the Innsbruck Quartzphyllite. The mineral assemblage is muscovite (Ms) + chlorite (Chl) + quartz (Qz) + accessories (apatite Ap, rutile Rt). All mineral abbreviations are according to Whitney and Evans (2010)

and contain many vesicles which clearly indicate a high-temperature overprint while other, less reactive domains, still show the primary foliation. Most of the micas show bloated structures. The minerals in the foamy patches experienced the highest temperatures, which resulted in the formation of high-*T* minerals (olivine, spinel) and melt (Fig. 3). The pyrometamorphic rocks mostly contain the mineral assemblage olivine + orthopyroxene + plagioclase + spinel + glass. During the investigation an apatite-rich domain was found in which P-rich phases occur (Fig. 4). Elongated crystals of plagioclase dominate the texture of the micro-domain between these laths the assemblage tri-calcium phosphate phase (TCP) + phosphoran olivine occurs (Fig. 5).

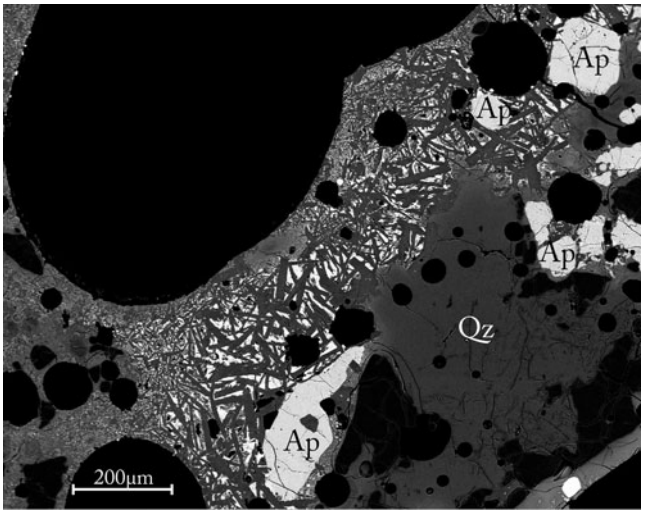


**Fig. 4** BSE overview image of the phosphorus domain adjacent to quartz (Qz). In close vicinity to apatite (Ap) anorthite (dark laths), phosphoran olivine and tri-calcium phosphate (bright crystals) occur. The black circular objects are vesicles. All mineral abbreviations are according to Whitney and Evans (2010)

## Analytical methods

*Electron microprobe analysis (EMPA)* A JEOL 8100 SUPERPROBE electron microprobe was used at the Institute of Mineralogy and Petrography of the University of Innsbruck. For a preliminary identification of minerals the energy dispersive spectrometer (Thermo Noran EDS system) was applied. The measurements were made using five wavelength-dispersive spectrometers (TAB, PETJ, PETH, LIF and LIFH). Measurement conditions were 15 kV acceleration voltage and a sample current of 10 nA. The measurement time was 20 s for the peak and 10 s for each site of the background positions. The beam size was 1 µm and for corrections the Phi-Rho-Z method was used (Pouchou and Pichoir 1984a, b). Standardization was done using natural and synthetic standards. In order to minimize the loss of volatile elements such as K and Na, a defocused beam with a diameter of 5 µm was used for mica and feldspar analysis. Mineral formulae were calculated using the program NORM-II by Ulmer (1993).

*Micro-Raman spectroscopy* The experimental setup of the micro-Raman spectroscopy was as follows: confocal Raman spectra were obtained with a HORIBA JOBIN YVON LabRam-HR 800 µ-Raman spectrometer at the Institute of Mineralogy and Petrography of the University of Innsbruck. Samples were excited at room temperature with the 532 and 633 nm emission line of a 100 mW Nd-YAG and a 17 mW

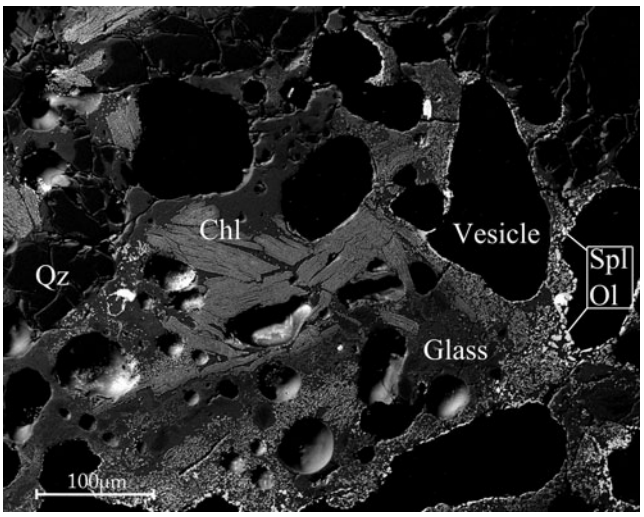


**Fig. 3** BSE image of a slag sample of the Innsbruck Quartzphyllite. In the upper section relicts of chlorite (Chl) are preserved within glass and on the right side olivine (Ol) and spinel (Spl) occur around vesicles. All mineral abbreviations are according to Whitney and Evans (2010)

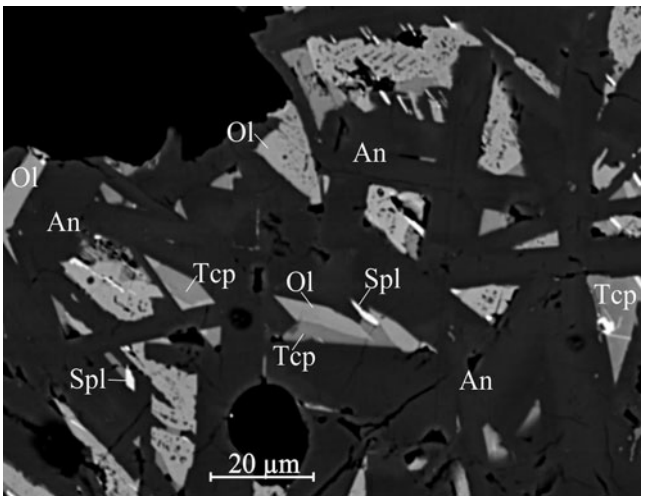


**Fig. 5** BSE close-up of the phosphorous domain. Tri-calcium phosphate (Tcp) and phosphoran olivine (Ol) crystallized as interstitial phases between An-rich plagioclase (An) laths. Spinel (Spl) also occurs. All mineral abbreviations are according to Whitney and Evans (2010) except for Tcp

He-Ne-laser, respectively, and an OLYMPUS 100X objective. The laser spot on the surface had a diameter of approximately 1 μm and a power of about 1 to 5 mW. Light was dispersed by a holographic grating with 1800 grooves/mm. Spectral resolution of about 1.8 $cm^{-1}$ was experimentally determined by measuring the Rayleigh line. The dispersed light was collected by a 1024×256 open electrode CCD detector. Confocal pinhole was set to 400 μm, resulting in a depth resolution of about 2–3 μm. Several spectra of single crystals were recorded without polarizers for the exciting laser and the scattered Raman light. The spectra were baseline-corrected by subtracting a squared polynomial function and fitted to Voigt functions. Peak shifts were calibrated by regular adjusting the zero-order position of the grating and controlled by measuring the Rayleigh line of a (100) polished single crystal silicon-wafer. Accuracy of Raman peak shifts was better than 0.5 $cm^{-1}$. The detection range was 100–1200 $cm^{-1}$. For phase identification the CrystalSleuth software and the RRUFF spectral database was used (Downs 2006).

## Mineral chemistry

*Quartzphyllite protolith* Muscovite from the western part of the Innsbruck Quartzphyllite complex shows a higher Si content of 3.07–3.29 apfu. than in the eastern part which has 3.06–3.17 apfu. (Piber 2005). In the unreacted samples from the immolation place muscovites have Si contents between 3.24 and 3.31 apfu. The chlorites from the western and the eastern part of the Innsbruck Quartzphyllite complex can also be distinguished. The $Fe^{2+}$ contents of chlorites from the western part are between 2.18 and 2.71 apfu and the Mg contents are between 1.69 and 2.38 apfu. (Piber 2005). The resulting $Fe^{2+}/(Fe^{2+}+Mg)$ ratio is 0.48–0.61. Chlorites from the eastern part of the Innsbruck Quartzphyllite complex show higher $Fe^{2+}$ contents with 2.72–2.91 apfu. and lower Mg contents of 1.47–1.62 apfu. (Piber 2005). The measured chlorites from the Goldbichl site have $Fe^{2+}$ contents between 2.24 and 2.34 apfu and Mg contents between 2.10 and 2.19 apfu., which yields $Fe^{2+}/(Fe^{2+}+Mg)$ ratios of 0.51–0.52. The Si contents vary little between 2.72 and 2.79 apfu. Plagioclase shows low anorthite ($X_{An}$) contents of 0.22 to 0.26, albite ($X_{Ab}$) contents of 0.77 to 0.73 albite and a K-feldspar component <0.1. Clinozoisite has $Fe^{3+}$ contents of 0.3 to 0.37 apfu. and rarely zoisite occurs with 0.09 apfu. $Fe^{3+}$. Rarely occurring garnet has a composition of $Alm_{43–53}Grs_{34–43}Pyr_{3–5}Sps_{4–10}$. Electron microprobe data of selected minerals of the protolith quartzphyllites are shown in Table 1.

*The P-rich domain* The olivines outside the P-rich domain show $X_{Fe}$ contents ranging from 0.44 to 0.84 (Table 2). Olivines within the P-rich domain contain an extraordinary high amount of P of up to 23 wt.% $P_2O_5$ as shown in Table 3. Although the whole domain is well crystallized the crystals are very small and only olivines with a sufficient size of 5–10 μm were selected to avoid contamination effects from the surrounding matrix. Since contamination from underlying feldspar and/or TCP cannot be ruled out completely, it was attempted to identify positive correlations between selected elements by plotting Ca + Mg + Fe vs. P which showed that the P-olivine analyses do not lie along a mixing line towards the TCP. Also no contamination from feldspar was observed since olivines contain almost no Ca and Al (Fig. 6a, b). In a Si vs. P plot the phosphoran olivines show a perfect correlation (Fig. 7). The P content strongly varies but reaches a maximum of 0.536 apfu. Figure 8 shows that not only the Si content decreases with increasing P contents but also the sum of cations on the $M_{1,2}$ positions decreases down to 1.655 apfu. The formula of olivine illustrates the strong compositional variations: $Mg_{0.584–0.978}Fe_{0.768–1.116}Mn_{0.011–0.022}Ca_{0.004–0.014}P_{0.289–0.536}Si_{0.480–0.777}O_4$. No chemical zoning was observed in olivine. Boesenberg and Hewins (2010) postulated the following charge balancing scheme for P incorporation in olivine:

$$2^{IV}Si^{+4} + 4^{VI}M^{+2} \leftrightarrow 3^{VI}M^{+2} + 2^{IV}P^{+5} + {}^{VI}\square$$

Rearrangement of their charge-balancing scheme leads to the more simplified charge balance scheme according to Tropper et al. (2004):

$$2Si^{4+} + {}^{VI}M^{2+} \leftrightarrow 2P^{5+} + {}^{VI}\square$$

In contrast to the data of Agrell et al. (1998) no substitution involving a tetrahedral vacancy such as

$$5Si^{4+} \leftrightarrow 4P^{5+} + {}^{IV}\square$$

was observed in the olivines of this investigation.

In the course of this investigation, a tri-calcium phosphate phase (TCP) was found. Chemically its composition fits several Ca-phosphates, namely graftonite (Ca, Mg, $Fe^{2+}$, $Mn^{2+}$)$_3$($PO_4$)$_2$, beusite ($Mn^{2+}$, $Fe^{2+}$, Ca, Mg)$_3$($PO_4$)$_2$, and stanfieldite $Ca_4$(Mg, $Fe^{2+}$, $Mn^{2+}$)$_5$($PO_4$)$_6$. Stanfieldite has been described from stony-iron meteorites (Fuchs 1967) as well as pallasites (Buseck and Holdsworth 1977) and often occurs coexisting with OH-free withlockite $Ca_3(PO_4)_2$ or farringtonite $Mg_3(PO_4)_2$ (Steele and Olson 1992). None of these phases have been found in the P-rich domain. Graftonite is known from pegmatites and meteorites (Floss 1999) and it shows complete miscibility with beusite, which represents the Mn end-member (Hurlbut and Aristarain 1968). The TCP from the P-rich domain has a high content of Fe, Ca and especially Mg, which is in good agreement with the chemical composition of stanfieldite as reported by Fuchs (1967) in Table 4. The Ca contents of 3.41 to 3.83 apfu are lower than in the ideal stanfieldite formula

**Table 1** Representative electron microprobe analyses of selected minerals of the western Innsbruck Quartzphyllite

| Sample | Chlorite-1 | Chlorite-3 | Muscovite-2 | Muscovite-4 | Feldspar-1 | Feldspar-3 |
|---|---|---|---|---|---|---|
| $SiO_2$ | 25.81 | 26.39 | 49.39 | 48.97 | 63.15 | 62.37 |
| $TiO_2$ | 0.04 | 0.07 | 0.18 | 0.21 | n.d. | n.d. |
| $Al_2O_3$ | 21.81 | 21.69 | 29.04 | 29.48 | 22.86 | 23.23 |
| $Cr_2O_3$ | 0.01 | 0.03 | 0.01 | 0.05 | n.d. | n.d. |
| FeO | 26.35 | 25.45 | 2.33 | 2.29 | 0.04 | 0.08 |
| MnO | 0.37 | 0.37 | n.d. | 0.03 | n.d. | n.d. |
| MgO | 13.56 | 13.4 | 2.42 | 2.25 | 0.04 | n.d. |
| CaO | n.d. | n.d. | 0.03 | n.d. | 4.89 | 4.91 |
| $Na_2O$ | 0.02 | 0.04 | 0.22 | 0.11 | 9.20 | 9.34 |
| $K_2O$ | n.d. | 0.28 | 10.64 | 10.77 | 0.11 | 0.09 |
| Total | 87.96 | 87.71 | 94.26 | 94.16 | 100.29 | 100.02 |
| Basis: | (a) | (a) | (b) | (b) | (c) | (c) |
| Si | 2.721 | 2.779 | 3.318 | 3.293 | 2.785 | 2.753 |
| Ti | 0.003 | 0.005 | 0.009 | 0.011 | n.d. | n.d. |
| $Al^{IV}$ | 1.279 | 1.221 | 0.682 | 0.707 | 1.188 | 1.209 |
| $Al^{VI}$ | 1.43 | 1.471 | 1.617 | 1.629 | n.c. | n.c. |
| Cr | <0.001 | 0.002 | <0.001 | 0.003 | n.d. | n.d. |
| $Fe^{3+}$ | n.c. | n.c. | 0.101 | 0.110 | 0.001 | 0.003 |
| $Fe^{2+}$ | 2.323 | 2.241 | 0.03 | 0.019 | n.c. | n.c. |
| Mn | 0.033 | 0.033 | n.d. | 0.001 | n.d. | n.d. |
| Mg | 2.131 | 2.104 | 0.242 | 0.226 | 0.002 | n.d. |
| Ca | n.d. | n.d. | 0.002 | n.d. | 0.231 | 0.232 |
| Na | 0.002 | 0.004 | 0.029 | 0.015 | 0.787 | 0.799 |
| K | n.d. | 0.019 | 0.912 | 0.924 | 0.006 | 0.005 |
| Sum | 9.921 | 9.88 | 6.943 | 6.937 | 4.999 | 4.999 |
| | | | | Anorthite | 0.226 | 0.224 |
| | | | | Albite | 0.768 | 0.771 |
| | | | | Orthoclase | 0.006 | 0.005 |

Calculation on the basis of a) 14 oxygens, b) 11 oxygens and c) 5 cations and 16 charges; *n.d.* not detected, *n.c.* not calculated; calculation of $Fe^{3+}$ is based on charge balance considerations

by Fuchs (1967) but similar to the analysis by Buseck and Holdsworth (1977) who report Ca contents down to 3.69 apfu. Nonetheless the data indicate a substitution of Fe and Mg for Ca since Ca and Mg, Fe and Mn show a strong linear negative correlation as shown in Fig. 9. Literature data show that this substitution can be up to 15 % for TCP as reported by Enderle et al. (2005) and Araujo et al. (2009). One analysis shows very small Ca contents of 2.82 apfu and since it still lies on the correlation line it might reflect an even stronger substitution. Compared to graftonite and beusite, the TCP shows much higher CaO (17–26 wt.% vs. 6–9 wt.% vs. 4.6–16.1 wt.%) and MgO (9–14 wt.% vs. 0.1–0.4 wt.% vs. <2.6 wt.%) concentrations. Therefore based on the observed chemical composition the TCP is most likely stanfieldite (Table 4).

Spinel is a solid solution between spinel-magnetite-hercynite-magnesioferrite and ulvöspinel as shown in Table 5. The feldspar laths are plagioclase with higher K contents than plagioclase from the protolith (Table 6). This could be due to the breakdown of muscovite, which releases K. The feldspars laths from the P-rich domain contain higher anorthite contents with the following formula: $Ab_{0.42–0.54}An_{0.32–0.52}$ $Or_{0.07–0.21}$. These plagioclases also contain about 0.6 wt.% $P_2O_5$ and hence the chemical composition of newly grown plagioclase strongly depends on the micro-domain in which they grew. Melt compositions outside the P-rich domains is peraluminous and also vary strongly in composition, due to its formation in different micro-domains (Table 7). Melt compositions could only be measured outside the P-rich domains due to the small grain size and thus no P contents were detected in the melt. Due to the high degree of crystallization no melt was observed in the P-rich domain. Minor orthopyroxene can be found in the slags as well as in the P-rich domain. The P-bearing orthopyroxenes vary strongly in their composition and all show a high Al component of 3–6 wt.% $Al_2O_3$ (Table 8). Al is incorporated on the tetrahedral position due to the Tschermaks substitution ($2Al^{3+} \leftrightarrow Si^{4+} + M^{2+}$). The $P_2O_5$ content is around 0.5 wt.% except for one orthopyroxene which contains 5.0 wt.% $P_2O_5$ which represents 0.16 apfu. P. This

**Table 2** Representative electron microprobe analyses of P-free olivine

| Sample | Gb1-ol1 | Gb1-ol2 | Gb1-ol4 | GB4-Ol1 | GB4-Ol2 | GB4-Ol5 |
|---|---|---|---|---|---|---|
| $SiO_2$ | 33.27 | 31.47 | 35.96 | 36.28 | 35.64 | 35.43 |
| $TiO_2$ | n.d. | n.d. | 0.15 | 0.21 | 0.05 | 0.07 |
| $Al_2O_3$ | 1.11 | 0.13 | 0.12 | 0.79 | 0.10 | 0.08 |
| FeO | 58.20 | 61.02 | 39.91 | 36.13 | 36.35 | 36.19 |
| MnO | 1.04 | 1.59 | 0.96 | 0.39 | 0.49 | 0.52 |
| MgO | 6.14 | 5.56 | 24.88 | 24.74 | 25.46 | 25.24 |
| CaO | 0.46 | 0.26 | 0.41 | 0.08 | 0.11 | 0.11 |
| $Na_2O$ | 0.05 | n.d. | n.d. | 0.02 | n.d. | n.d. |
| $K_2O$ | 0.01 | 0.01 | 0.02 | 0.30 | 0.09 | 0.06 |
| Total | 100.27 | 100.04 | 102.40 | 98.94 | 98.29 | 97.70 |
| Si | 1.063 | 1.020 | 0.999 | 1.033 | 1.020 | 1.021 |
| Ti | n.d. | n.d. | 0.003 | 0.005 | 0.001 | 0.001 |
| Al | 0.042 | 0.005 | 0.004 | 0.027 | 0.004 | 0.003 |
| $Fe^{2+}$ | 1.556 | 1.654 | 0.928 | 0.861 | 0.870 | 0.872 |
| Mn | 0.028 | 0.044 | 0.023 | 0.010 | 0.012 | 0.013 |
| Mg | 0.293 | 0.269 | 1.031 | 1.051 | 1.087 | 1.084 |
| Ca | 0.016 | 0.009 | 0.012 | 0.002 | 0.003 | 0.003 |
| Na | 0.003 | n.d. | n.d. | 0.001 | n.d. | n.d. |
| K | n.d. | <0.001 | <0.001 | 0.011 | 0.003 | 0.002 |
| Sum | 3.000 | 3.000 | 3.000 | 3.000 | 3.000 | 3.000 |
| $X_{Mg}$ | 0.15 | 0.14 | 0.52 | 0.53 | 0.55 | 0.55 |
| $X_{Fe}$ | 0.80 | 0.84 | 0.46 | 0.44 | 0.44 | 0.44 |

Calculation on the basis of 3 cations, *n.d.* not detected

**Table 3** Representative electron microprobe analyses of phosphoran olivines of the P-rich domain

| | P-Ol-1 | P-Ol-2 | P-Ol-3 | P-Ol-4 | P-Ol-5 | P-Ol-6 | P-Ol-7 |
|---|---|---|---|---|---|---|---|
| $SiO_2$ | 22.75 | 17.58 | 21.93 | 21.21 | 19.39 | 21.7 | 21.22 |
| $TiO_2$ | 0.22 | 0.15 | 0.17 | 0.22 | 0.08 | 0.06 | 0.15 |
| $Al_2O_3$ | 0.06 | 0.07 | 0.15 | 0.15 | 0.12 | 0.08 | 0.2 |
| $P_2O_5$ | 14.95 | 23.18 | 16.9 | 17.84 | 21.86 | 18.76 | 17.34 |
| $Cr_2O_3$ | 0.05 | n.d. | 0.04 | 0.03 | 0.06 | n.d. | n.d. |
| FeO | 45.1 | 38.26 | 42.44 | 41.14 | 37.91 | 34.32 | 44.21 |
| MnO | 0.81 | 0.93 | 0.86 | 0.8 | 0.7 | 0.49 | 0.92 |
| MgO | 15.9 | 19.35 | 17.42 | 18.26 | 18.95 | 24.53 | 15.64 |
| CaO | 0.29 | 0.29 | 0.46 | 0.14 | 0.33 | 0.45 | 0.18 |
| $Na_2O$ | 0.04 | 0.05 | 0.05 | 0.05 | 0.04 | 0.04 | 0.02 |
| $K_2O$ | 0.02 | 0.05 | 0.05 | 0.03 | 0.02 | 0.01 | 0.09 |
| Total | 100.18 | 99.91 | 100.45 | 99.87 | 99.44 | 100.44 | 99.97 |
| Si | 0.650 | 0.480 | 0.614 | 0.592 | 0.530 | 0.580 | 0.602 |
| Ti | 0.005 | 0.003 | 0.004 | 0.005 | 0.002 | 0.001 | 0.003 |
| Al | 0.002 | 0.002 | 0.005 | 0.005 | 0.004 | 0.003 | 0.007 |
| P | 0.361 | 0.536 | 0.400 | 0.422 | 0.506 | 0.425 | 0.416 |
| Cr | 0.001 | n.d. | 0.001 | 0.001 | 0.001 | n.d. | n.d. |
| $Fe^{2+}$ | 1.077 | 0.873 | 0.993 | 0.960 | 0.866 | 0.768 | 1.049 |
| Mn | 0.020 | 0.022 | 0.020 | 0.019 | 0.016 | 0.011 | 0.022 |
| Mg | 0.677 | 0.787 | 0.727 | 0.760 | 0.772 | 0.978 | 0.661 |
| Ca | 0.009 | 0.008 | 0.014 | 0.004 | 0.010 | 0.013 | 0.006 |
| Na | 0.002 | 0.003 | 0.002 | 0.003 | 0.002 | 0.002 | 0.001 |
| K | 0.001 | 0.002 | 0.002 | 0.001 | 0.001 | <0.001 | 0.003 |
| ∑ cations $M_{1,2}$ | 1.773 | 1.682 | 1.740 | 1.739 | 1.655 | 1.757 | 1.732 |
| ∑ all cations | 2.804 | 2.715 | 2.781 | 2.771 | 2.709 | 2.781 | 2.769 |

Calculation on the basis of 4 oxygens, *n.d.* not detected

amount of P can only be accommodated by the substitution of P and Al instead of Si on the tetrahedral site according to the following vector (Boesenberg and Hewins 2010):

$$P^{5+} + Al^{3+} \leftrightarrow 2\ Si^{4+}$$

## Micro-Raman-spectroscopy

P-bearing olivine and P-free olivine were measured with micro-Raman spectroscopy and measurements of P-bearing olivine were difficult to obtain due to the extremely small grain size (<20 μm, Fig. 5). The P-free olivine shows a spectrum comparable to fayalite with in total 14 bands and the most intense bands around 846 and 817 $cm^{-1}$, as shown in Fig. 10. Weaker bands occur at 1183, 1113, 937, 909, 877, 590, 569, 419, 334, 296, 197 and 135 $cm^{-1}$. The high wavenumber bands at 937, 846 and 817 $cm^{-1}$ can be assigned to internal stretching vibrations of the $SiO_4$-tetrahedron (Chopelas 1991). The two bands above 1100 $cm^{-1}$ are very weak and might be related to inclusions or impurities whereas the low-wavenumber bands are probably caused by external vibrations of the tetrahedron and the $M_1$ and $M_2$ octahedrons. The phosphoran olivine was measured at two different wavelengths (633 and 532 nm) and shows in total 20 bands: three intense one at 936, 832 and 822 $cm^{-1}$ and weaker bands at 1096, 1049, 975, 725, 680, 631, 582, 561, 510, 457, 405, 368, 331, 291, 228, 163 and 113 $cm^{-1}$. Above 965 $cm^{-1}$ no bands are observed in olivines and, with the exception of monticellite, above 900 $cm^{-1}$ they are generally very weak (Chopelas 1991). The intense band at 936 $cm^{-1}$ and the high wavenumber bands are therefore rather assigned to the internal symmetric stretching of a $PO_4$ tetrahedron (Fig. 10). This might be caused by a vacancy in the $M_1$ and $M_2$ sites, generated by the incorporation of P, which Boesenberg and Hewins (2010) attributed to distortions in the olivine structure due to a change towards farringtonite. The fine-grained nature of the material prevented more-detailed Raman investigations. Comparison of the phosphoran olivine spectra with the RRUFF spectra database (Downs 2006), which contains at present more than 5000 Raman spectra of minerals, yielded only poor matches, thus confirming the results of the mineral-chemical investigations.

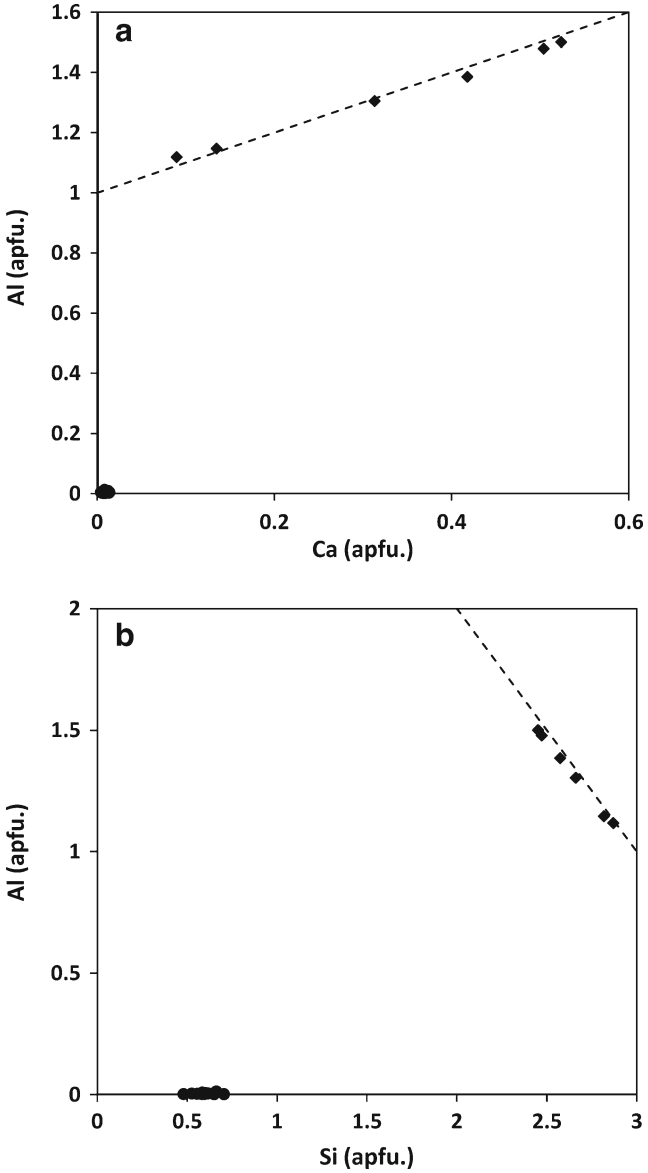


**Fig. 6** Correlation diagrams between Ca vs. Al (**a**) and Si vs. Al (**b**) to illustrate a possible chemical contamination from adjacent anorthite laths (*diamonds*). The phosphoran olivines are represented by the *black circles*. The amounts of Si, Ca and Al are too low and thus no chemical mixing trend involving anorthite could be observed. The *dashed lines* represent the compositional trends in the feldspars

Micro-Raman investigations of the TCP yielded 18 bands, three intense one at 983, 974 and 968 $cm^{-1}$ and a large number of weaker bands at 176, 293, 348, 402, 468, 514, 533, 611, 620, 753, 1075, 1124, 1158, 1228 and 1293 $cm^{-1}$. The three most intense bands again are probably related to the internal stretching vibration of the $PO_4$ tetrahedron. No conclusive match with a spectrum from the RRUFF database could be obtained so far (Downs 2006). Figure 11 shows the Raman spectra of the TCP compared to the spectra of graftonite, beusite and sarcopside, all from the RRUFF database. Although the TCP shows a composition that is very similar

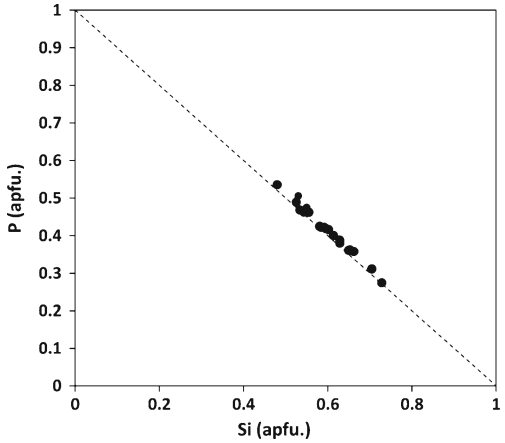


**Fig. 7** Linear correlation between Si and P (apfu.) in the phosphoran olivine of the samples from the immolation place. The dashed line represents the 1:1 P substitution for Si according to the charge balance scheme $2Si^{4+}+{}^{VI}M^{2+} \leftrightarrow 2P^{5+}+{}^{VI}\square$

to graftonite, the graftonite Raman spectrum does not match. This is also the case with the structurally-related spectrum of beusite $(Ca_{1.818}Mg_{0.516}Fe^{2+}_{0.560}Mn_{0.022})_{2.916}(PO_4)_{2.001}$ from the Bull Moose Mine, Custer, South Dakota, USA. Another TCP, sarcopside $(Fe^{2+}_{2.30}Mn_{0.67}Mg_{0.03})(PO_4)_2$, shows a similar most intense band at ca. 970 $cm^{-1}$ but also a second most intense band at 925 $cm^{-1}$, which clearly deviates from the obtained TCP pattern., The chemical data of TCP match with stanfieldite, unfortunately, no Raman spectrum of this mineral for comparison is available so far.

## Discussion

*Textural evolution of the slags* At atmospheric pressure minerals start changing their shape due to the rising temperatures.

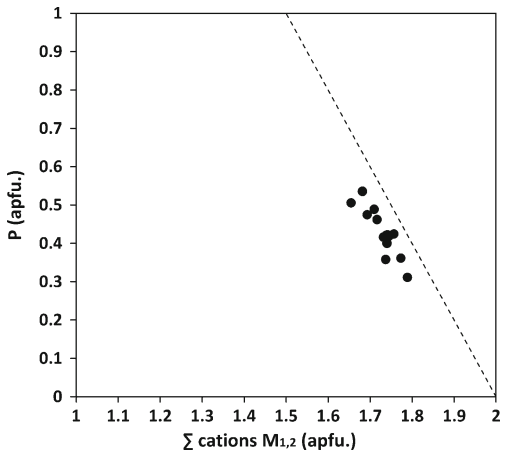


**Fig. 8** Correlation between P and the sum of $M_{1,2}$ cations in the phosphoran olivines. The dashed line represents the correlation between the vacancies in $M_{1,2}$ and the P content according to the charge balance scheme $2Si^{4+}+{}^{VI}M^{2+} \leftrightarrow 2P^{5+}+{}^{VI}\square$. Note that the phosphoran olivines are slightly shifted towards lower $M_{1,2}$ values

**Table 4** Representative electron microprobe analyses of stanfieldite

| | TCP-2 | TCP-3 | TCP-4 | TCP-5 | Stanfieldite |
|---|---|---|---|---|---|
| $P_2O_5$ | 45.33 | 46.29 | 45.52 | 46.25 | 46.6 |
| CaO | 26.19 | 21.42 | 17.01 | 23.46 | 24.6 |
| MgO | 9.10 | 13.82 | 14.43 | 11.33 | 12.9 |
| FeO | 18.26 | 17.46 | 21.11 | 19.14 | 13.8 |
| MnO | 0.68 | 0.69 | 0.99 | 0.77 | 1.4 |
| $SiO_2$ | 0.24 | 0.42 | 0.15 | 0.39 | n.d. |
| $Al_2O_3$ | 0.10 | 0.13 | 0.08 | 0.07 | n.d. |
| $Cr_2O_3$ | n.d. | 0.04 | n.d. | n.d. | n.d. |
| $TiO_2$ | 0.02 | 0.02 | 0.04 | 0.06 | n.d. |
| $K_2O$ | 0.06 | 0.05 | 0.10 | 0.06 | n.d. |
| $Na_2O$ | 0.14 | 0.07 | 0.17 | n.d. | n.d. |
| Total | 100.06 | 100.36 | 99.5 | 101.47 | 99.3 |
| P | 5.982 | 5.955 | 5.957 | 5.964 | 6.00 |
| Ca | 3.406 | 3.488 | 2.817 | 3.829 | 4.02 |
| Mg | 3.221 | 3.131 | 3.325 | 2.573 | 2.91 |
| Fe | 2.198 | 2.219 | 2.729 | 2.438 | 1.74 |
| Mn | 0.101 | 0.089 | 0.130 | 0.099 | 0.18 |
| Si | 0.048 | 0.064 | 0.023 | 0.059 | n.d. |
| Al | 0.011 | 0.023 | 0.015 | 0.013 | n.d. |
| Cr | n.d. | 0.003 | n.d. | n.d. | n.d. |
| Ti | <0.001 | 0.005 | 0.009 | 0.014 | n.d. |
| K | 0.008 | 0.005 | 0.010 | 0.006 | n.d. |
| Na | 0.021 | 0.010 | 0.025 | n.d. | n.d. |
| Sum | 14.974 | 14.992 | 15.039 | 14.995 | 14.85 |

Calculation of the stanfieldite formula on the basis of 24 oxygens; *n.d.* not detected. Stanfieldite analysis from Fuchs (1967)

**Table 5** Representative electron microprobe analyses of spinel

| Sample | Gb1-sp1 | Gb1-sp2 | Gb1-sp3 | Gb1-sp4 | Gb1-sp5 |
|---|---|---|---|---|---|
| $SiO_2$ | 0.58 | 0.24 | 1.29 | 0.36 | 0.29 |
| $TiO_2$ | 0.16 | 0.09 | 28.85 | 1.38 | 0.12 |
| $Al_2O_3$ | 49.08 | 54.27 | 1.90 | 13.59 | 13.00 |
| $Cr_2O_3$ | 0.06 | 0.11 | 0.83 | 0.04 | 0.02 |
| $Fe_2O_3$ | 11.35 | 6.21 | 8.13 | 60.72 | 64.65 |
| FeO | 36.57 | 36.78 | 54.71 | n.d. | 0.52 |
| MnO | 0.31 | 0.47 | 0.96 | 1.69 | 1.02 |
| MgO | 2.43 | 2.40 | 1.68 | 23.00 | 20.9 |
| CaO | 0.06 | 0.07 | 0.56 | 0.16 | 0.12 |
| $Na_2O$ | 0.02 | 0.03 | 0.12 | n.d. | n.d. |
| $K_2O$ | n.d. | n.d. | 0.06 | 0.06 | 0.09 |
| Total | 100.62 | 100.67 | 99.09 | 101.02 | 100.77 |
| Si | 0.017 | 0.007 | 0.047 | 0.011 | 0.009 |
| Ti | 0.004 | 0.002 | 0.794 | 0.032 | 0.003 |
| Al | 1.706 | 1.847 | 0.082 | 0.485 | 0.473 |
| Cr | 0.001 | 0.003 | 0.024 | 0.001 | 0.001 |
| $Fe^{3+}$ | 0.252 | 0.135 | 0.224 | 1.383 | 1.503 |
| $Fe^{2+}$ | 0.902 | 0.888 | 1.674 | n.d. | 0.014 |
| Mn | 0.008 | 0.012 | 0.030 | 0.043 | 0.027 |
| Mg | 0.107 | 0.103 | 0.092 | 1.038 | 0.962 |
| Ca | 0.002 | 0.002 | 0.022 | 0.005 | 0.004 |
| Na | 0.001 | 0.002 | 0.009 | n.d. | n.d. |
| K | n.d. | n.d. | 0.003 | 0.002 | 0.004 |
| Sum | 2.999 | 2.998 | 2.997 | 3.000 | 2.999 |
| $MgAl_2O_4$ | 0.092 | 0.096 | 0.020 | 0.256 | 0.230 |
| $FeAl_2O_4$ | 0.767 | 0.822 | 0.019 | 0.000 | 0.002 |
| $MnAl_2O_4$ | 0.007 | 0.011 | 0.006 | 0.011 | 0.006 |
| $MgFe_2O_4$ | 0.014 | 0.007 | 0.053 | 0.730 | 0.732 |
| $FeFe_2O_4$ | 0.114 | 0.060 | 0.051 | 0.000 | 0.006 |
| $MnFe_2O_4$ | 0.001 | 0.001 | 0.018 | 0.030 | 0.020 |
| $MgCr_2O_4$ | n.c. | n.c. | 0.005 | 0.001 | 0.000 |
| $FeCr_2O_4$ | 0.001 | 0.001 | 0.005 | 0.000 | 0.000 |
| $MnCr_2O_4$ | n.c. | n.c. | 0.002 | 0.000 | 0.000 |
| $Fe_2TiO_4$ | 0.004 | 0.002 | 0.822 | 0.031 | 0.003 |

Calculation on the base of 3 cations and 8 charges, *n.d.* not detected; *n.c.* not calculated, calculation of $Fe^{3+}$ is based on charge balance considerations. The $SiO_2$ contents are most likely due to contamination from adjacent silicates

The sheet silicates such as chlorite and muscovite react during heating with intensified bloating and microcracking due to dehydration of adhesive and of structurally bound water (Grapes 2006). Until the α–β transition of quartz at 575 °C the dilation occurs moderately and continuously (Grapes 2006). Vitrification occurs at a temperature of ≈900 °C while degasification channels and bloating structures are produced at temperatures ≈1200 °C (Grapes 2006). During firing of the quartzphyllites the micas break down along a continuous process, beginning with substantial water loss. The original textures of muscovite and chlorite are preserved only as relicts and at higher firing temperatures small cubic crystals of spinel form within the chlorite

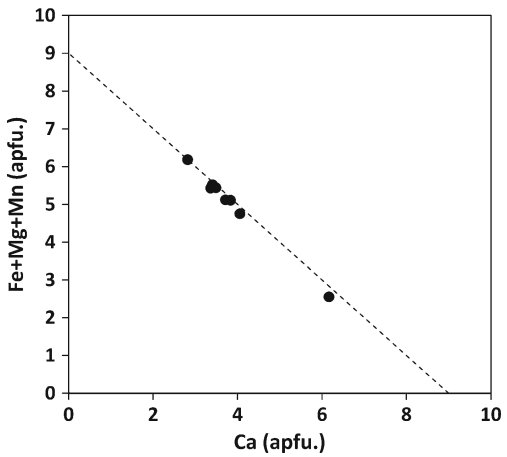


**Fig. 9** Ca vs. Fe + Mg + Mn correlation in stanfieldite $Ca_4(Mg, Fe^{2+}, Mn^{2+})_5(PO_4)_6$

**Table 6** Representative electron microprobe analyses of feldspar from the P-rich domain

| Sample | Gb1-An-4 | P-An-10 | P-An-12 | P-An15 | P-An16 | P-An-22 | P-An-39 |
|---|---|---|---|---|---|---|---|
| $SiO_2$ | 58.41 | 63.26 | 54.63 | 55.07 | 59.27 | 62.43 | 57.8 |
| $TiO_2$ | 0.11 | 0.19 | 0.06 | 0.07 | 0.12 | 0.13 | 0.06 |
| $Al_2O_3$ | 24.98 | 20.92 | 28.36 | 27.94 | 24.65 | 21.56 | 26.40 |
| $P_2O_5$ | 0.59 | 0.63 | 0.66 | 0.48 | 0.64 | 0.64 | 0.67 |
| $Cr_2O_3$ | n.d. | 0.02 | n.d. | n.d. | n.d. | n.d. | n.d. |
| $Fe_2O_3$ | 0.35 | n.c. | n.c. | 0.34 | n.c. | n.c. | n.c. |
| FeO | n.c. | 0.38 | 0.37 | n.c. | 0.24 | 0.65 | 0.26 |
| MnO | n.d. | 0.01 | n.d. | 0.03 | n.d. | 0.04 | n.d. |
| MgO | 0.04 | n.d. | 0.08 | 0.06 | 0.05 | 0.07 | 0.04 |
| CaO | 7.76 | 1.85 | 10.89 | 10.48 | 6.51 | 2.79 | 8.76 |
| $Na_2O$ | 6.43 | 3.32 | 4.74 | 5.08 | 5.46 | 3.78 | 5.99 |
| $K_2O$ | 1.67 | 10.12 | 1.14 | 1.17 | 3.59 | 8.90 | 1.17 |
| Total | 100.41 | 100.7 | 100.93 | 100.71 | 100.53 | 100.99 | 101.16 |
| Si | 2.615 | 2.869 | 2.452 | 2.472 | 2.661 | 2.816 | 2.573 |
| Ti | 0.004 | 0.006 | 0.002 | 0.002 | 0.004 | 0.005 | 0.002 |
| Al | 1.318 | 1.118 | 1.5 | 1.478 | 1.304 | 1.147 | 1.385 |
| P | 0.023 | 0.024 | 0.025 | 0.018 | 0.024 | 0.025 | 0.025 |
| Cr | n.d. | 0.001 | n.d | n.d | n.d | n.d | n.d |
| $Fe^{3+}$ | 0.012 | n.c | n.c | 0.011 | n.c | n.c | n.c |
| $Fe^{2+}$ | n.c. | 0.015 | 0.014 | n.c | 0.009 | 0.024 | 0.01 |
| Mn | n.d. | <0.001 | n.d | 0.001 | n.d | 0.001 | n.d |
| Mg | 0.003 | n.d | 0.005 | 0.004 | 0.004 | 0.005 | 0.003 |
| Ca | 0.372 | 0.09 | 0.524 | 0.504 | 0.313 | 0.135 | 0.418 |
| Na | 0.558 | 0.292 | 0.413 | 0.442 | 0.475 | 0.331 | 0.517 |
| K | 0.095 | 0.585 | 0.065 | 0.067 | 0.206 | 0.512 | 0.067 |
| Sum | 5.000 | 5.000 | 5.000 | 5.000 | 5.000 | 5.000 | 5.000 |
| Anorthite | 0.36 | 0.093 | 0.523 | 0.497 | 0.315 | 0.138 | 0.417 |
| Albite | 0.54 | 0.302 | 0.412 | 0.436 | 0.478 | 0.338 | 0.516 |
| K-feldspar | 0.09 | 0.605 | 0.065 | 0.066 | 0.207 | 0.524 | 0.066 |

Calculation on the base of 5 cations and 16 charges, *n.d.* not detected; *n.c.* not calculated; calculation of $Fe^{3+}$ is based on charge balance considerations

layers (Fig. 3). Depending on the distance to the fire different temperatures and oxygen conditions affected the rocks. The highest temperature was at the contact area between the rock and the fire where the most obvious melting processes took place. In these areas high temperature led to the breakdown of the initial assemblage muscovite + chlorite + plagioclase + quartz ± biotite ± clinozoisite ± ilmenite to the formation of the new pyrometamorphic assemblage: plagioclase (an-rich) + olivine + spinel + melt ± orthopyroxene due to the following model reactions involving the breakdown of chlorite:

$$\text{Chlorite} \rightarrow 2\,\text{Olivine} + \text{Spinel} + \text{Quartz} + 4\,H_2O$$
$$\text{Chlorite} \rightarrow \text{Olivine} + \text{Spinel} + 2\,\text{Orthopyroxene} + 4\,H_2O$$

Orthopyroxene can also form due to a reaction between olivine and quartz and occurs therefore in an advanced stage of pyrometamorphism (Grapes 2006). Adjacent to olivine, large blades of plagioclase crystallized. Between the plagioclase crystals isometric crystals of ulvospinel occur (Fig. 3). Biotite is rare so the main source of Ti in these rocks is titanite. The proposed model reaction involving chlorite and titanite thus could be:

**Table 7** Representative electron microprobe analyses of melt

| | Melt-1 | Melt-3 | GB1-Melt-1 |
|---|---|---|---|
| $SiO_2$ | 49.84 | 66.51 | 48.12 |
| $Al_2O_3$ | 31.96 | 18.13 | 34.04 |
| $Na_2O$ | 2.75 | 3.86 | 3.68 |
| $K_2O$ | 6.04 | 6.71 | 1.02 |
| CaO | 0.84 | 1.12 | 11.07 |
| FeO | 4.93 | 1.99 | 1.50 |
| MgO | 2.57 | 0.52 | 1.28 |
| $TiO_2$ | 0.33 | n.d. | 0.10 |
| MnO | 0.05 | 0.02 | 0.05 |
| Total | 99.31 | 98.90 | 100.86 |

**Table 8** Representative electron microprobe analyses of orthopyroxene

| Sample | Gb1-Px1 | Gb1-Px2 | Gb1-Px3 | Gb1-Px4 |
|---|---|---|---|---|
| $SiO_2$ | 49.46 | 45.97 | 51.02 | 41.11 |
| $TiO_2$ | 1.56 | 3.02 | 1.45 | 2.05 |
| $Al_2O_3$ | 6.05 | 4.87 | 3.36 | 5.71 |
| $Cr_2O_3$ | n.d. | 0.05 | 0.20 | n.d. |
| $P_2O_5$ | 0.57 | 0.55 | 0.03 | 5.00 |
| FeO | 28.10 | 28.21 | 21.18 | 28.26 |
| MgO | 13.25 | 15.69 | 21.51 | 16.46 |
| MnO | 0.78 | 0.67 | 0.54 | 0.39 |
| CaO | 0.76 | 1.05 | 1.81 | 0.54 |
| $Na_2O$ | 0.19 | 0.10 | 0.07 | 0.08 |
| $K_2O$ | 0.58 | 0.13 | n.d. | 0.04 |
| Total | 101.29 | 100.31 | 101.17 | 99.65 |
| Si | 1.876 | 1.779 | 1.882 | 1.590 |
| Ti | 0.045 | 0.088 | 0.040 | 0.060 |
| Al | 0.270 | 0.222 | 0.146 | 0.260 |
| Cr | n.d. | 0.002 | 0.006 | n.d. |
| P | 0.018 | 0.018 | 0.001 | 0.164 |
| $Fe^{2+}$ | 0.891 | 0.913 | 0.653 | 0.914 |
| Mg | 0.749 | 0.905 | 1.183 | 0.949 |
| Mn | 0.025 | 0.022 | 0.017 | 0.013 |
| Ca | 0.031 | 0.043 | 0.072 | 0.023 |
| Na | 0.007 | 0.004 | 0.003 | 0.003 |
| K | 0.014 | 0.003 | n.d. | 0.001 |
| Sum | 3.927 | 3.998 | 4.002 | 3.976 |

Calculation on the base of 6 oxygens, *n.d.* not detected

2 Chlorite + 4 Titanite →
Olivine + 2 Anorthite + 4 Ulvospinel + 5 Quartz
+ 8 $H_2O$ + $O_2$

In muscovite-rich domains, only the formation of peraluminous melt was observed.

*The composition of phosphoran olivines and structural constraints* Previous descriptions of the occurrence of phosphoran olivines indicates that they grew under strongly disequilibrium conditions and P substitution for Si in olivine is not surprising since several phosphates with olivine-like structures exist (e.g., Eventoff et al. 1972; Nord and Stefanidis 1983; Chung et al. 2002; Langer et al. 2006, 2007). Chemical data from naturally occurring phosphoran olivines indicate that in these samples the maximum P content is 0.13 apfu whereas synthetic olivines from experimental investigations contain considerably higher P-contents. For instance the experimental data of Boesenberg and Hewins (2010) yielded the maximum P-content of 0.68 apfu in olivine, which implies P contents of up to 27 wt.% $P_2O_5$. This is equivalent to a tetrahedral site occupancy of P of ca. 70 %, which is thought be represent the maximum value based upon structural considerations in the system forsterite-farringtonite, $Mg_2SiO_4$-$Mg_3(PO_4)_2$ since the ratio Si:P is 1:2 (Boesenberg and Hewins 2010). The data from this study show maximum contents of 23 wt.% $P_2O_5$, which is equivalent to 54 % P substitution for Si. The data of this study, and the data from Tropper et al. (2004), Boesenberg et al. (2004) and Boesenberg and Hewins (2010) lie nicely along the 1:1 P → Si correlation line. With respect to the nature of the olivine-phosphate phase solid solution, several possibilities for olivine-phosphate solid solutions exist.

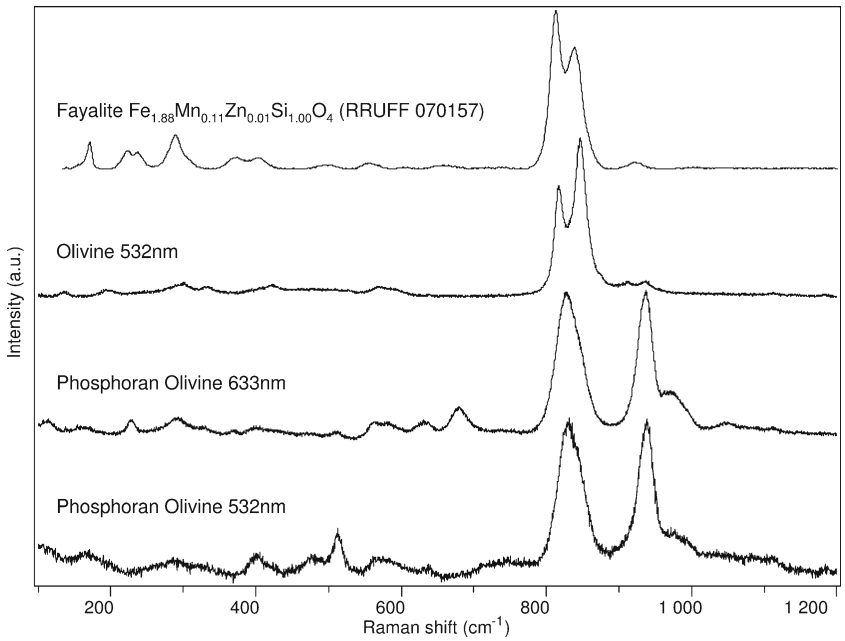


**Fig. 10** Raman spectra of olivines. Top: Raman spectrum of fayalite from the RRUFF database (Downs 2006). Second from the top: Raman spectrum of P-free olivine from a slag sample. The lower two spectra are from a phosphoran olivine, excited at 633 and 532 nm (bottom)

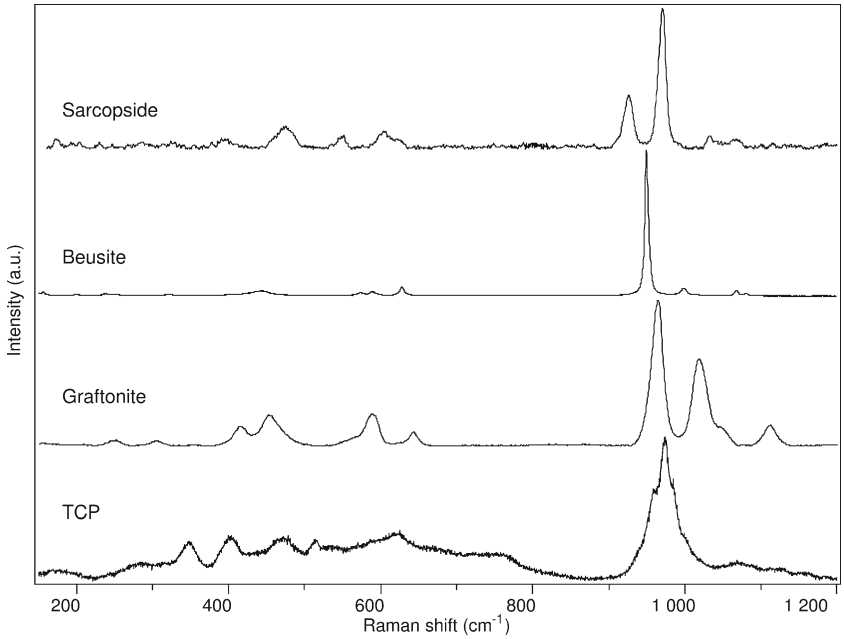


**Fig. 11** Raman spectra of selected phosphate phases. Top: RRUFF database spectrum of sarcopside ($Fe^{2+}_{2.30}Mn_{0.67}Mg_{0.03}(PO_4)_2$. Second from top: beusite ($Fe^{2+}$,$Mn^{2+}$, $Ca)_3(PO_4)_2$, from the Bull Moose Mine, Custer, South Dakota, USA. Third from top: RRUFF database spectrum of graftonite ($Fe^{2+}$, $Mn^{2+}$, Mg, $Ca)_3(PO_4)_2$. The lowermost spectrum represents the Raman spectrum of a TCP from the P-rich domain in the slag. All spectra were excited at 532 nm

The structure of farringtonite ($Mg_3(PO_4)_2$ is closely related to the structure of forsterite, but shows monoclinic instead of orthorhombic symmetry. Similar to olivine the three-dimensional framework of farringtonite is composed of $PO_4$-tetrahedra that are linked together by metal-oxide polyhedra. There are also two sites $M_1$ and $M_2$, which are five- and six-fold coordinated ($MgO_5$ i.e., $MgO_6$) according to Nord and Kierkegaard (1968). But even more closely related to the olivine structure are the phosphate minerals sarcopside ($Fe_3(PO_4)_2$, Moore 1972) and its Mg-rich counterpart chopinite ($Mg_3(PO_4)_2$, Grew et al. 2007) which also have an olivine-type structure with hexagonal closest oxygen package. Brunet and Vielzeuf (1996) and Brunet et al. (1998) showed that chopinite ($Mg_3(PO_4)_2$-II) is a high-pressure polymorph of farringtonite and they predicted that $Fe^{2+}$ would stabilize chopinite-sarcopside solid solutions towards lower pressures, which may indicate that the P-bearing olivines from this study could be a ternary solid solution between fayalite-chopinite-sarcopside. Metastable chopinite-sarcopside solid solutions have been reported by Grew et al. (2010) in meteorites, but clearly more experimental and structural investigations in the systems $Mg_3(PO_4)_2$-$Mg_2SiO_4$ and $Fe_3(PO_4)_2$-$Fe_2SiO_4$ under anhydrous conditions are needed in order to deduce the exact nature of this olivine-phosphate-type solid solution.

*Theoretical phase relations involving phosphoran olivines in pyrometamorphic quartzphyllites* In this investigation, it is thought that phosphoran olivine formed by pyrometamorphic reactions between apatite, chlorite, plagioclase and quartz from mineral assemblage of the quartzphyllite during immolation. Investigations on the phase relationships in the system CaO-FeO-$SiO_2$-$P_2O_5$-$Al_2O_3$-$H_2O$ with the phases chamosite-quartz-fayalite-anorthite-hercynite-apatite-sarcopside-$H_2O$ allow to infer the conditions of formation as a function of $T$ and $aSiO_2$ as shown in Fig. 12. The following Schreinemakers diagram (Fig. 12) is based on two major assumptions: 1.) only the olivine Fe-end-member system was considered, and 2.) in order to account for the incorporation of P into olivines the Fe-endmember sarcopside, $Fe_3(PO_4)_2$, was used since it is stable at atmospheric pressures and has an olivine-type structure (Moore 1972). The following reactions intersect in an invariant

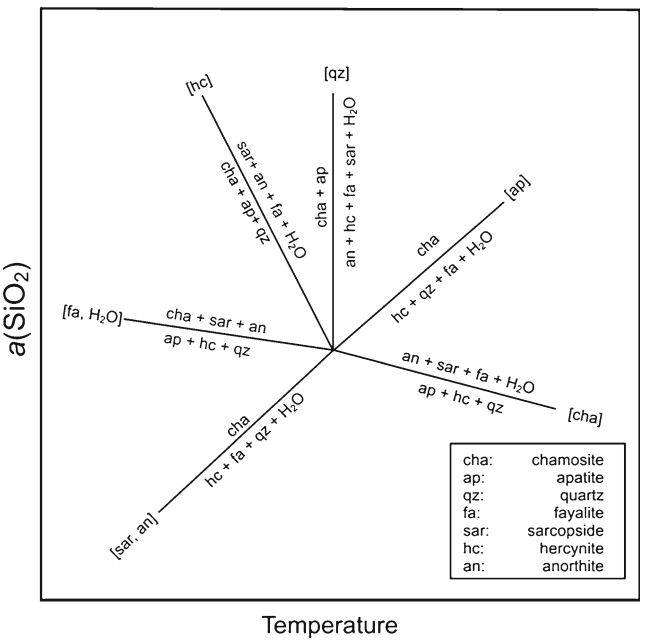


**Fig. 12** Schreinemakers diagram depicting the $T$-log$aSiO_2$-space at constant $fH_2O$. The observed phase assemblage olivine + anorthite + Fe-phosphate (sarcopside) lies in the upper part of the diagram stretching between the hercynite- and chamosite-absent reactions [hc] and [cha] at high $T$ and $aSiO_2$ conditions

point and occur at $O_2$-fugacities below the QFM-buffer. The absent phases are given in brackets.

1.) 10 Chamosite + 2 Apatite + 10.5 Quartz →3 Sarcopside +10 Anorthite + 20.5 Fayalite + 41$H_2O$ [Hc]

2.) Chamosite → Quartz + Hercynite + 2 Fayalite + 4$H_2O$ [Ap]

3.) Chamosite → Quartz + Hercynite + 2 Fayalite + 4$H_2O$ [An, Sar]

4.) 2 Apatite + 10 Hercynite + 20.5 Quartz → Anorthite+ 3 Sarcopside + 0.5 Fayalite + $H_2O$ [Cha]

5.) Chamosite + 40 Anorthite + 12 Sarcopside → 8Apatite +41 Hercynite + 83 Quartz [Fa, $H_2O$]

6.) 20 Chamosite + 2 Apatite →3Sarcopside + 10 Anorthite +10 Hercynite + 40.5 Fayalite + 81$H_2O$ [Qtz]

Mineral reactions involving chamosite and apatite and forming fayalite-sarcopside solid solutions (reactions 1 and 6) strongly depend on the presence of quartz. Reaction 1 leads to the phase assemblage sarcopside + fayalite + anorthite, which occurs in the high-*T*/high $aSiO_2$ portion of the diagram in Fig. 12 and which can also be observed in the P-rich domains of the slags. Since most reactions considered are dehydration reactions the exact positions of the equilibria are also strongly dependent on $fH_2O$, which can be quite high during the initial stages of dehydration (Grapes 2006). Therefore for a quantitative evaluation of these equilibria this diagram needs to be extended into 3 dimensions by also considering changing $fH_2O$ and thus the invariant point will become a line.

## Conclusions and archaeological implications

The chemical varability of the phases formed in the slags during the ritual immolation process and the occurrence of extensive P-substitution in olivine strongly indicate disequilibrium growth in relatively $SiO_2$-rich domains due to rapid quenching. This is consistent with the implications associated with phosphoran olivine growth in natural occurrences (Buseck and Clark 1984; Agrell et al. 1998; Goodrich 1984; Brunet and Chazot 2000) and in a ritual immolation site (Tropper et al. 2004), as well as in experimental investigations (Konzett et al. 2002; Boesenberg et al. 2004; Boesenberg and Hewins 2010; Tropper et al. 2006).

Experimental investigations of Konzett et al. (2002) and Tropper et al. (2006) have shown that the interaction between bone material and biotite-plagioclase gneisses during partial melting lead to the formation of the assemblage phosphoran olivine + whitlockite + plagioclase + clinopyroxene + glass, which is similar to the assemblage observed in the slags found in Oetz. Based on this observation Tropper et al. (2004) suggested that the identification of mineral assemblages such as phosphoran olivines + whitlockite in partially molten rocks from firing sites could indeed provide mineralogical evidence for the identification of ritual immolation sites, in case archaeological artefacts have not been found. On the other hand, preliminary investigations by Schneider (2009) and the results from this investigation show that the occurrence of phosphoran olivine is restriced to extremely P-rich domains and thus is only related to the presence of accessory apatite in the slag and that phosphoran olivines can form due to the breakdown of apatite as shown by model reactions in Fig. 12. In addition the extent of P-substitution in olivine is also much higher compared to Oetz, which might be due to the Ca-poor nature of these quartzphyllites, which is reflected in the formation of orthopyroxene rather than clinopyroxene and which seems to favor the formation of sarcopside-fayalite solid solutions.

The formation of P-rich olivine from accessory apatite is thus in contrast to the investigations by Tropper et al. (2004) who proposed that bone-rock interactions alone are responsible for the formation of phosphoran olivines. This fact might also be reflected by the presence of a different phosphate phase in the slag samples from the Goldbichl. In this investigation a TCP phase (stanfieldite) instead of whitlockite was found. Therefore caution is advised concerning the archaeological implications of the occurrence of phosphoran olivine in slags from ritual immolation sites, since it can also form without the presence of bone material.

**Acknowledgments** Financial support through the FWF special research program HiMAT (F3110-G02 to P.T.) is gratefully acknowledged. Thanks to Bernhard Sartory for his help with the microprobe. The helpful reviews of F. Brunet of an earlier version of the manuscript and two anonymous journal reviewers are also greatly appreciated.

## References

Agrell SO, Charnley NR, Chinner A (1998) Phosphoran olivine from Pine Canyon, Piute Co., Utah. Mineral Mag 62:265–269

Araujo JC, Sader MS, Moreia EL, Moraes VCA, LeGeros RZ, Soares GA (2009) Maximum substitution of magnesium for calcium sites in Mg-β-TCP structure determined by X-ray powder diffraction with the Rietveld refinement. Mat Chem Phys 118:337–340

Boesenberg JS (2006) Wrought iron from the USS monitor: mineralogy, petrology and metallography. Archaeometry 48:613–631

Boesenberg JS, Hewins RH (2010) An experimental investigation into the metastable formation of phosphoran olivine and pyroxene. Geochim Cosmochim Acta 74:1923–1941

Boesenberg JS, Ebel RH, Hewins RH (2004) An experimental study of phosphoran olivine and its significance in main group pallasites. Lunar Planet Sci Conf XXXV, Lunar Planet. Inst., Houston:#1368 (abstract)

Brunet F, Chazot G (2000) Partioning of phosphorus between olivine, clinopyroxene and silicate glass in a spinel lherzolite xenolith from Yemen. Chem Geol 176:51–72

Brunet F, Vielzeuf D (1996) The farringtonite/$Mg_3(PO_4)_2$-II transformation: a new curve for pressure calibration in pistoncylinder apparatus. Eur J Mineral 8:349–354

Brunet F, Chopin C, Seifert F (1998) Phase relations in the MgO-$P_2O_5$-$H_2O$ system and the stability of phosphorellenbergerite: petrological implications. Contrib Mineral Petrol 131:54–70

Buseck PR, Clark J (1984) Zaisho - a Pallasite Containing Pyroxene and Phosphoran Olivine. Mineral Mag 48:229–235

Buseck PR, Holdsworth E (1977) Phosphate minerals in pallasite meteorites. Mineral Mag 41:91–102

Chlingensperg M (1904) Der Knochenhügel am Langacker und die vorgeschichtliche Herdstelle am Eisenbichl bei Reichenhall in Oberbayern. Mitt Anthrop Ges Wien 34:53–70

Chopelas A (1991) Single crystal Raman spectra of forsterite, fayalite, and monticellite. Am Mineral 76:1101–1109

Chung SY, Bloking JT, Chiang YM (2002) Electronically conductive phosphor-olivines as lithium storage electrodes. Nat Mater 1:123–128

Downs RT (2006) The RRUFF Project: an integrated study of the chemistry, crystallography, Raman and infrared spectroscopy of minerals. Progr Abstr 19th Gen Meet Intern Mineral Assoc, Kobe, Japan

Enderle R, Götz-Neunhoeffer GM, Müller FA, Greil P (2005) Influence of magnesium doping on the phase transformation temperature of β-TCP ceramics examined by Rietveld refinement. Biomaterials 26:3379–3384

Eventoff W, Martin R, Peacor DR (1972) The crystal structure of heterosite. Am Mineral 57:45–51

Floss C (1999) Fe, Mg, Mn-bearing phosphates in the GRA 95209 meteorite: occurrences and mineral chemistry. Am Mineral 84:1354–1359

Fuchs LH (1967) Stanfieldite: a new phosphate mineral from stony-iron meteorites. Science 158:910–911

Gleirscher P, Nothdurfter H, Schubert E (2002) Das Rungger Egg. Röm-German Forsch, Verlag Philipp von Zabern, Mainz 61, pp. 264

Goodrich CA (1984) Phosphoran pyroxene and olivine in silicate inclusions in natural iron-carbon alloy, Disko Island, Greenland. Geochim Cosmochim Acta 48:2769–2771

Grapes RH (2006) Pyrometamorphism. Springer, Berlin, p 275

Grew ES, Armbruster T, Medenbach O, Yates MG, Carson CJ (2007) Chopinite, [(Mg, Fe)$_3$⑨](PO4)2, a new mineral isostructural with sarcopside, from a fluorapatite segregation in granulite-facies paragneiss. Larsemann Hills, Prydz Bay, East Antarctica. Eur J Mineral 19:229–245

Grew ES, Yates MG, Beane RJ, Floss C, Gerbi C (2010) Chopinite-sarcopside solid solution, [(Mg, Fe)$_3$⑨](PO4)2, in GRA95209, a transitional acapulcoite: implications for phosphate genesis in meteorites. Am Mineral 95:260–272

Haditsch JG, Mostler H (1982) Zeitliche und stoffliche Gliederung der Erzvorkommen im Innsbrucker Quarzphyllit. Geol Paläont Mitt 12:1–40

Heimann R, Kreher U, Oexele J, Hirsekom V, Ullrich O, Janke D, Ullrich B, Lindner H, Wagenbreth B (1998) Archaeometallurgical investigations into the iron production technology in Upper Lusatia, Saxony, from the early Iron Age (Billendorf period) to the 12th century A.D. Eur J Mineral 10:1015–1035

Hurlbut CS, Aristarain LF (1968) Beusite, a new mineral from Argentina, and the graftonite-beusite series. Am Mineral 53:1799–1814

Konzett J, Tropper P, Recheis A (2002) Experimental investigations onthe formation of phosphoran olivine in partially molten gneisses from aprehistoric sacrificial place, Tyrol, Austria. Jour Conf Abstr 7:58

Langer K, Taran MN, Fransolet AM (2006) Electronic absorption spectra of phosphate minerals with olivine-type structures: I. Members of the triphylite-lithiophilite series, $^{M1[6]}Li^{M2[6]}(Fe_{x2+}Mn_{1-x}^{2+})[PO_4]$. Eur J Mineral 18:337–344

Langer K, Taran MN, Fransolet AM (2007) Electronic absorption spectra of phosphate minerals with olivine-type Structures: II. The oxidized minerals ferrisicklerite, $^{M1[6]}(⑨_{1-x}Li_x)^{M2[6]}(Fe^{3+}{}_{1-x}Mn^{2+}{}_x)[PO_4]$, and heterosite, $^{M1[6]}(⑨_{1.00})^{M2[6]}(Fe^{3+}{}_{1-x}Mn^{3+}{}_x)[PO_4]$, with x≤0.5. Eur J Mineral 19:589–592

Moore PB (1972) Sarcopside: its atomic arrangement. Am Mineral 57:24–35

Müller G, Schuster AK, Zippert Y (1988) Spinifex textures and texture zoning in fayalite-rich slags of medieval iron-works near Schieder Village, NW-Germany. N Jb Miner Monatsh 3:111–120

Nord AG, Kierkegaard P (1968) The crystal structure of $Mg_3(PO_4)_2$. Acta Chem Scand 22:1466–1474

Nord AG, Stefanidis T (1983) Crystallographic studies of some olivine-related (Ni, Mg)3(PO4)2 solid solutions. Phy Chem Mineral 10:10–15

Piber A (2005) The metamorphic evolution of the Austro-Alpine nappes north of the Tauern window (Innsbruck Quartzphyllite Complex - Patscherkofel Complex - Kellerjochgneiss and Wildschönau Schist). Unpubl Ph.D. Thesis, Univ Innsbruck: pp. 261

Pouchou JL, Pichoir F (1984a) A new model for quantitative X-ray-microanalysis. 1. Application to the analysis of homogenous samples. La Rech Aérospatiale 3:167–192

Pouchou JL, Pichoir F (1984b) A new model for quantitative X-ray-microanalysis. 2. Application to in-depth analysis of heterogenous samples. La Rech Aérospatiale 5:349–367

Schneider P (2009) Mineralogisch-petrologische Untersuchungen der Pyrometamorphose in Brandopferplätzen. Institut für Mineralogie und Petrographie. Unpubl MSc Thesis, Univ Innsbruck: pp. 124

Steele IM, Olson E (1992) Crystal structure of natural stanfieldite from the Imilac pallasite. Lun Planet Sci Conf Lun Planet Inst, Houston:#1355 (abstract)

Tomedi G, Nicolussi Castellan S (2000) Ein bronze- und eisenzeitlicher Brandopferplatz am Goldbichl bei Igls (Bez. Innsbruck-Stadt). ArchaeoTirol Kl Schrift 2:122–123

Tropper P, Recheis A, Konzett J (2004) Experimental investigations on the pyrometamorphic formation of phosphorous-bearing olivines in partially molten metapelitic gneisses. Eur J Mineral 16:631–640

Tropper P, Konzett J, Recheis A (2006) Experimental investigations on the pyrometamorphic formation of phosphorus-bearing olivines in partially molten metapelitic gneisses. Mitt Österr Mineral Ges 152:47–56

Ulmer P (1993) Norm-program for cation and oxygen mineral norms. Computer Library IKPETH, Zürich

Weiss RM (1997) Prähistorische Brandopferplätze in Bayern. Intern Archäo 35:203

Whitney DL, Evans BW (2010) Abbrevations for names of rock-forming minerals. Am Mineral 95:185–187